

Chapter 4

Effects of the Driver Switching Frequency on Performance of the Brushless Direct Current Motor

Buğra Er¹
Tuba Kocaer²
Çağlar Acar³
Ahmet Fenercioğlu⁴

¹ R&D Engineer; KORMAS Electric Motor Inc. TOSB OSB, Kocaeli,
bugraer@kormas.com ORCID No: 0000-0002-3982-5654

² R&D Engineer; KORMAS Electric Motor Inc. TOSB OSB, Kocaeli,
tubakocaer@kormas.com ORCID No: 0000-0003-4614-7158

³ R&D Engineer; KORMAS Electric Motor Inc. TOSB OSB, Kocaeli,
caglaracar@kormas.com ORCID No: 0000-0002-7849-4464

⁴ Prof. Dr.; Tokat Gaziosmanpaşa University, Department of Mechatronics Engineering, ahmet.fenercioglu@gop.edu.tr ORCID No: 0000-0002-1522-6868

1. INTRODUCTION

Brushless Direct Current Motor (BLDCM) has high starting torque and is frequently preferred in variable speed applications. Without brushes, mechanical wear, noise and temperature can be minimized. The control algorithm is quite complex compared to brushed DC motors. The rotor position must be detected and commutation must be performed. Hall effect sensors are used in sensor control to detect the rotor position. It is advantageous to use hall sensors in applications that need to be lifted under load. It triggers the appropriate phase by evaluating the data from three sensors for motor starting. Control of acceleration-related switching angles is mandatory. On the other hand, the acceleration rate also depends on the load characteristics. Reducing the start time depends on the characteristics of the driven load as well as the control method applied. Only when currents are controlled the motor speed will increase according to the mechanical dynamics of the system. By observing the BLDCM driver waveforms, the control characteristic that provides the optimum operating condition can be obtained. The BLDCM torque characteristic can then be optimized during operation by applying the appropriate, pre-calculated opening and closing angles according to the motor current and speed. With this control method, a trapezoidal signal will appear. The switching frequency effect on the driver circuit varies depending on the load and speed of the motor.

The BLDCM in Figure 1 and the driver in Figure 2 are shown. There are supply input, phase outputs, hall sensor supply, sensor inputs, and speed information input on the driver. Board structure is made of a microprocessor, MOSFET driver, MOSFET, and regulators. Necessary hardware calculations have been made.



Figure 1: BLDC Motor



Figure 2: BLDC

Motor Driver

In the study of Bekiroglu and Dalgin (2020), BLDCM speed and position controls were performed using an algorithm-based controller. Hall sensors are used to obtain the position data of the motor. The sensors are used to obtain the position data of the motor. Sinusoidal and trapezoidal reference models were

used in the control system. The proposed control system is operated for speed control as well as position control of the motor. The developed velocity and position control method have been tested for both trapezoidal and sinusoidal commutation techniques. The results obtained from these commutation techniques are compared. The speed and the position results of the motor were obtained under different load and operating conditions.

Papathanasopoulos et al (2020) proposed an alternative approach for reliable state monitoring of the BLDCM driver in critical applications. A data-driven approach to diagnosing unstable system operation is presented, with a focus on field-effect position sensor-based drives.

According to Zhang et al (2020), a driver controller of the brushless DC motor is designed in terms of hardware and software, according to the BLDCM specifications and working principle. STM32F103RBT6 is used as a microprocessor, including a control system, power supply circuit, driver circuit, and detection circuit. Su et al. (2019) study designed the control system with STM32 microprocessor as the core, including power circuit, driver isolation circuit, communication circuit, and protection circuit. The power supply and filter circuit are designed to increase the stability of the power supply by reducing the power supply ripple.

Pindoriya et al. (2018) carried out the design and application of a brushless direct current motor driver using FPGA. The FPGA drives a six-pulse three-phase inverter using the digital pulse width modulation control technique. This control strategy is simple and powerful, providing motor control without the need for a current sensor. The simulation of the proposed technique was performed using MATLAB/Simulink and the corresponding results were verified with the experimental results of the FPGA board.

Kolano et al. (2021) tried to reduce the negative effects in case of faulty performance or failure of the elements that determine the rotor position in the sensor control of the brushless motor. Ctibor et al. (2019) Brushless motor driver STM32 ARM microcontroller is used. It explained the application structure, the drivers and peripherals used, and the cascading control structure applied. Echle et al. (2020), a comparative analysis of BLDCM drive methods for an axial flux motor with a trapezoidal inverse-emf waveform is presented. It has shown that the BLDCM mode with 120-degree conduction has the best efficiency performance.

In this study, motor loading tests were carried out according to different switching frequencies. In these tests, the current, speed, efficiency, and power values of the motor were measured by applying torque to the motor at certain intervals from low load to overload under 13 V DC voltage. In the tests, the speed and current were interpreted at the same torque values by changing the switching frequency. According to the results obtained, improvements in 10 kHz and 15 kHz switching frequency values at different loads were determined by evaluating the brushless motor performance data. The motor driver has been optimized from 9 kHz to 15 kHz, resulting in better performance.

2. MATERIALS AND METHOD

BLDCM is electronically controlled due to its structure and rotor position information is required in the control process for correct current commutation. In this study, position information was obtained using hall sensors. In the control of brushless DC motors, two separate closed loops are used. The first is the internal control loop, where the motor current or torque is controlled. For this purpose, the currents of the motor phase windings are continuously monitored and the reference current is monitored. The second is the external control loop. In this cycle, the motor speed is controlled. As feedback, the actual motor speed and position information from the position sensors are processed in the Speed controller.

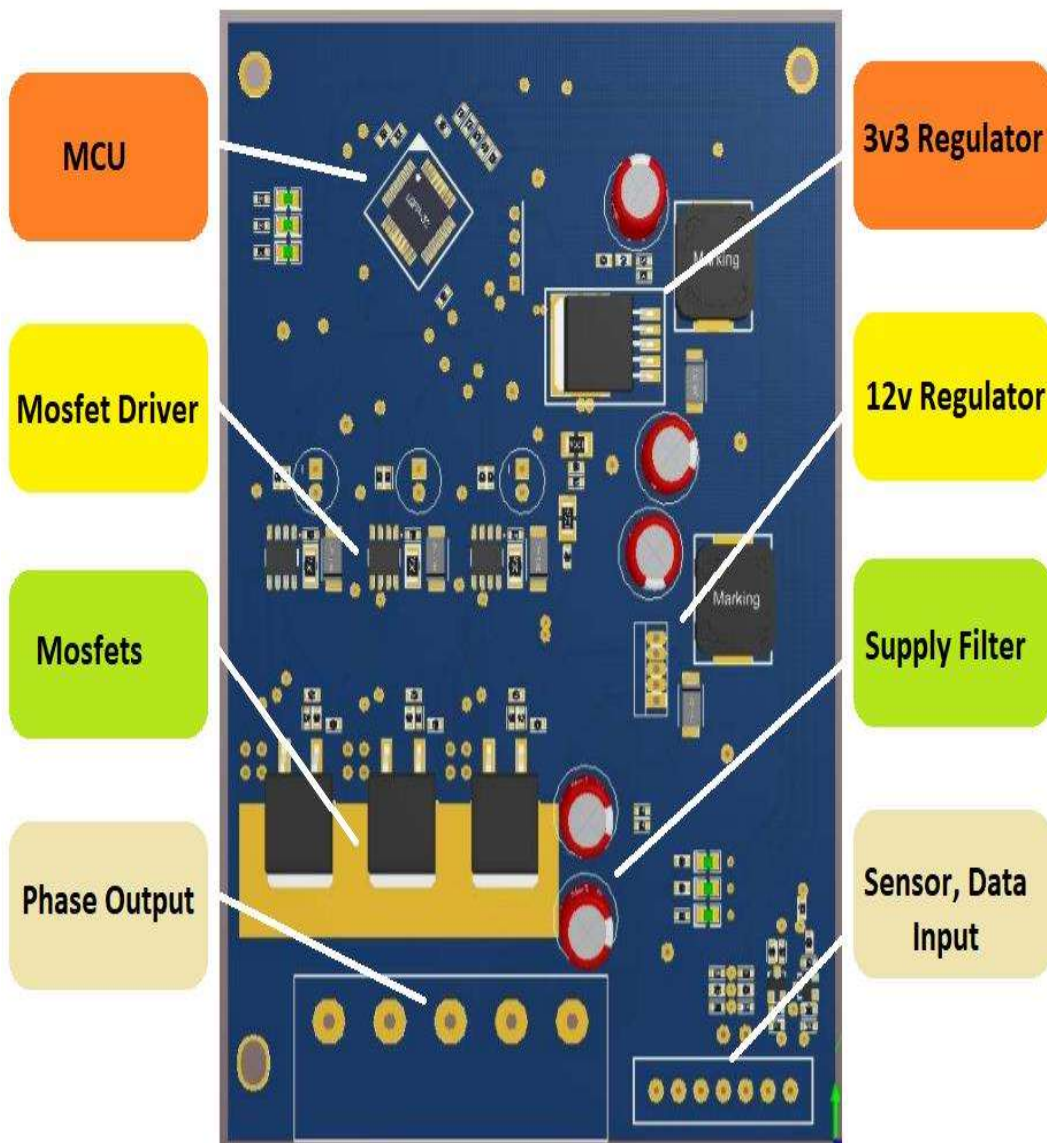


Figure 3: BLDCM driver partitions

There is a 3v3 regulator with the processor used in the STM32 series. The 3v3 regulator is also the supply of the hall effect sensors. 12v is used for MOSFET driver. The supply of the 3v3 regulator is taken from a 12V power source. MOSFETs and phase outputs are given. The voltage drop on the MOSFET gate is 12v, and a capacitor is used as the supply filter. The Hall effect sensor input and the functions performed on the driver, input of which is designed, are shown in Figure 3.

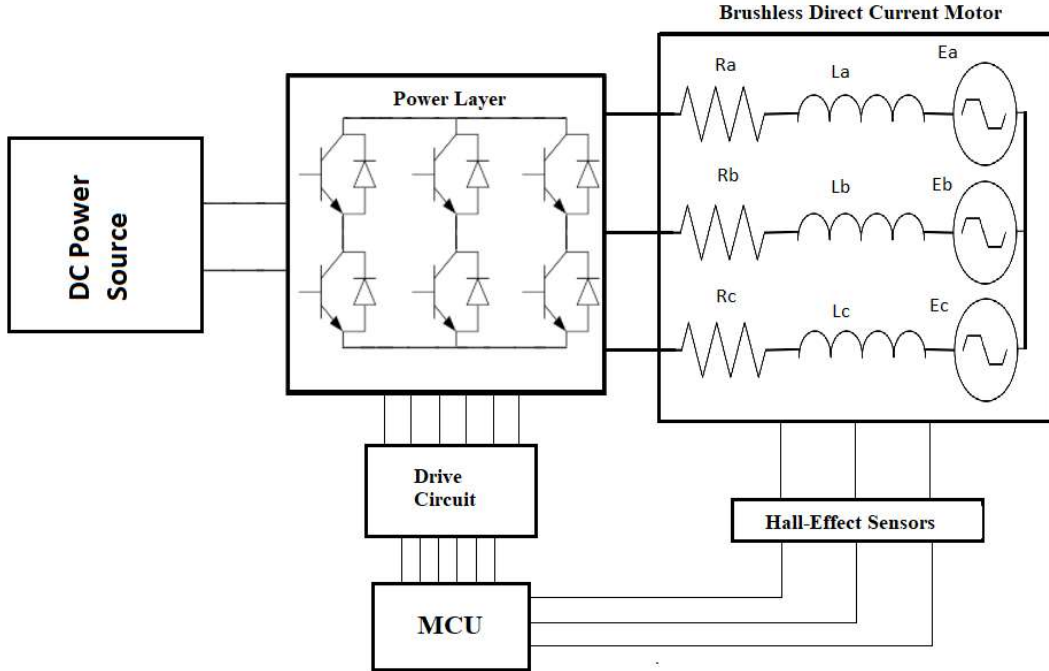


Figure 4: BLDCM driver schematic diagram

The schematic diagram of the BLDCM driver shown in Figure 4 is given. Assuming that the three-phase balanced systems operate at nominal current without any change in angle and rotor reluctance, the voltage equations are given with the equations (1), (2), (3).

$$V_a = R_a I_a + L_a \left(\frac{dI_a}{dt} \right) + E_a \quad (1)$$

$$V_b = R_b I_b + L_b \left(\frac{dI_b}{dt} \right) + E_b \quad (2)$$

$$V_c = R_c I_c + L_c \left(\frac{dI_c}{dt} \right) + E_c \quad (3)$$

Here; V_a, V_b, V_c Input phase voltages (V), I_a, I_b, I_c , Stator phase currents (A), E_a, E_b, E_c are back-EMF (V). $L_a = L_b = L_c = L_s$ are armature inductances in Henry and $R_a = R_b = R_c = R$ are armature resistance in ohms

In the first step of the BLDCM, the formulas included in the equations (1), (2), (3) were used depending on the resistance and inductance. The inductance on the armature is a time-dependent variable and is directly related to the switching frequency. The necessary features, mainly inductance, for the BLDCM studied are given in Table 1.

Table 1: 13v Brushless direct current motor features

| Parameter | Value | Unit |
|--------------------------------------|-----------|------|
| Nominal Speed | 4000 | Rpm |
| Nominal Voltage | 12 | V |
| Stator Winding Factor | 0,866025 | |
| D-Axis Reactive Inductance L_{ad} | 5395,06 | nH |
| Q- Axis Reactive Inductance L_{aq} | 5395,06 | nH |
| D- Axis Inductance L_1+l_{ad} | 27593,9 | nH |
| Q- Axis Inductance L_1+l_{aq} | 27593,9 | nH |
| Armature Leakage Inductance L_1 | 22198,9 | nH |
| Armature Phase Resistance R_1 | 0,0282124 | Ohm |
| D-Axis Time Constant (s) | 191230 | ns |
| Q-Axis Time Constant (s) | 191230 | ns |

The brushless DC motor has a permanent magnet rotor and the rotor position must be known for electronic commutation. The magnetic field is controlled by semiconductor elements that are switched according to the rotor position. In brushless DC motors, pole change is done electronically with semiconductor switches. The relevant phases to be triggered according to the sensor positions are given in Table 2. As a result of these triggers, the motor is driven together with the trapezoidal signal. In brushless DC motors, commutation consists of six steps. Each step corresponds to electrical intervals of 60 degrees and the two windings are energized. The rotor position determines the order of the switching steps. Therefore, knowing the rotor position is essential for control in brushless DC motors.

Table 2: Sensor locations and associated phases

| Hall-Effect Sensors | | | Phase Current | | |
|---------------------|----|----|---------------|-----|-----|
| HA | HB | HC | A | B | C |
| 1 | 0 | 1 | Off | - | + |
| 1 | 0 | 0 | + | - | Off |
| 1 | 1 | 0 | + | Off | - |
| 0 | 1 | 0 | Off | + | - |
| 0 | 1 | 1 | - | + | Off |
| 0 | 0 | 1 | Off | - | + |

The motor used in the study has 150 W mechanical power, 12/8 slot-pole combination, and 3500 rpm nameplate values and is used in a centrifugal pump drive. Torque tests of this motor were carried out with the help of the Festo DriveLab motor tester. The servo motor shaft in the Festo test system is connected to the test motor using a coupling. Servo motor applies a load to the test motor at specified intervals and torque test is performed by recording current, speed, operating voltage and applied load Torque of test motor.

Operated with 12V BLDCM driver. The behavior of the motor connected to the Festo Torque test measuring device under load was observed, graphics such as torque, speed, power, and efficiency of the motor were obtained and the operating curve of the motor was calculated. The torque test setup is given in Figure 5. Table 3, Table 4, and Table 5 show the variation of motor Torque test results according to frequency.

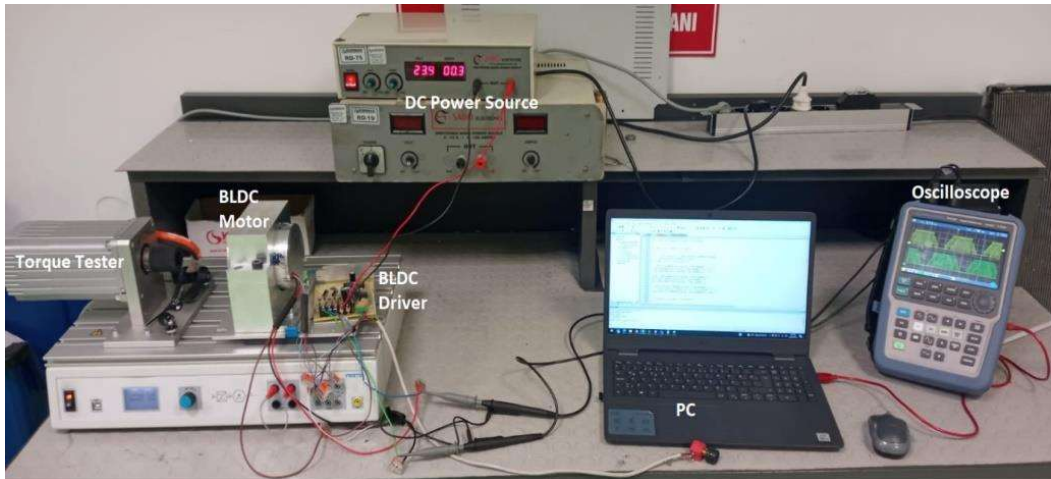


Figure 5: BLDCM loading test setup

Phase plots are taken with a pulse width modulated (PWM) signal with %50 occupancy to show frequency differences. Phase-Phase graphics of the motor are shown in Figure 6, which has a %94 occupancy rate. Rohde & Schwarz's interface was used to get the graphics from the oscilloscope screen. The switching frequency within the trapezoidal phase signal is expressed as frequency. Frequency differences are seen in the graphs. In Figure 7, Figure 8, Figure 9, and Figure 10, the number of switching on the trapezoidal phase signal is noticeable. Changing the switching frequency is achieved using a software provided by the Prescaler register. Switching frequency refers to the frequency within a certain phase signal. This directly affects the data depending on the inductance of the motor and the time constant. At the same time, if the frequency is the sound , change takes place.

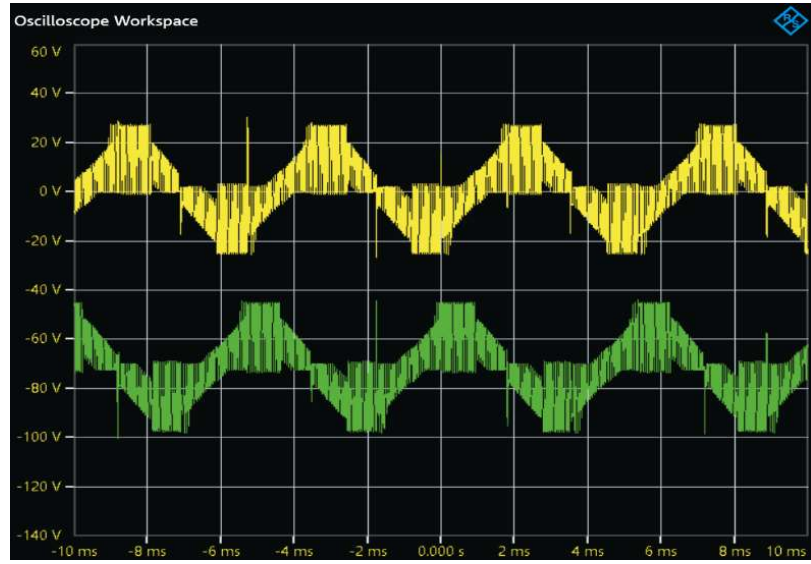


Figure 6: Phase-Phase graph

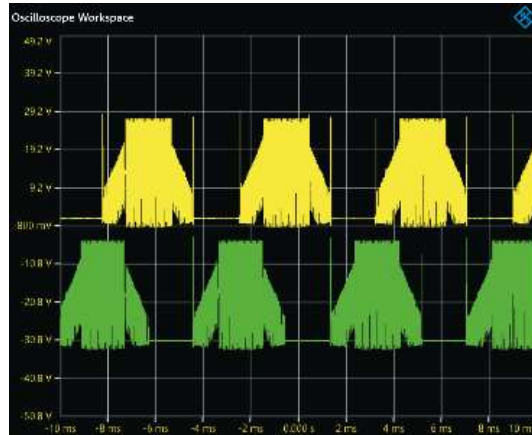


Figure 7: %50 PWM 20 kHz

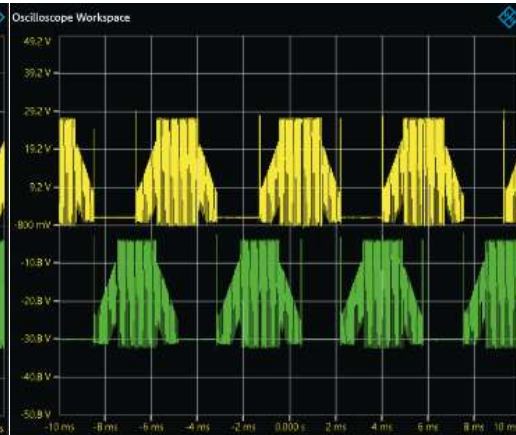


Figure 8: %50 PWM 15 kHz



Figure 9: %50 PWM 12 kHz

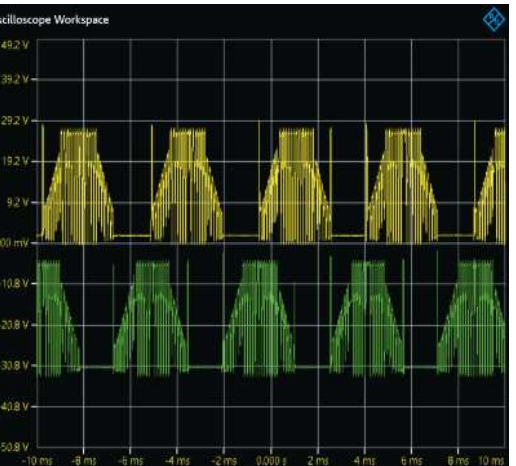


Figure 10: %50 PWM 8 kHz

As for switching frequency, there is a switching frequency that should be selected according to the coil inductance in the motor winding. In BLDCM driving, it has been determined to start as 9kHz and to reach steady as 15kHz. Due to the BLDCM load, relatively low frequency is preferred for starting. At its nominal speed, it was decided that 15 kHz was better. In the studies, the motor was loaded at 10 kHz-15 kHz-20 kHz switching frequencies. The output data was recorded as Table 3, Table 4 and Table 5 together with the output graphics.

As for switching frequency, there is a switching frequency that should be selected according to the coil inductance in the motor winding. It is determined that it starts from 9 kHz and reaches to 15 kHz in motor driving. Relatively low frequency is preferred for start-ups due to motor load. At its nominal speed, it was decided that 15 kHz was better.

Table 3: PWM frequency = 10 kHz

| Torque | Speed | Current | Voltage | P _{mec} | P _{elec} | Efficiency |
|---------|----------|---------|---------|------------------|-------------------|------------|
| 0,17 Nm | 3810 d/d | 8,1 A | 13 V | 105,30 W | 67,83 W | %64 |
| 0,27 Nm | 3590 d/d | 11,1 A | 13 V | 144,30 W | 101,51 W | %70 |
| 0,36 Nm | 3390 d/d | 13,6 A | 13 V | 175,44 W | 127,81 W | %74 |
| 0,45 Nm | 3170 d/d | 17,4 A | 13 V | 226,20 W | 149,39 W | %66 |
| 0,55 Nm | 3200 d/d | 19,4 A | 13 V | 265,78 W | 184,32 W | %69 |
| 0,63 Nm | 2470 d/d | 23,2 A | 13 V | 283,04 W | 162,96 W | %58 |

Table 4: PWM frequency = 15 kHz

| Torque | Speed | Current | Voltage | P _{mec} | P _{elec} | Efficiency |
|---------|----------|---------|---------|------------------|-------------------|------------|
| 0,17 Nm | 3860 d/d | 8,5 A | 13 V | 110,50 W | 68,72 W | %62 |
| 0,29 Nm | 3610 d/d | 11,8 A | 13 V | 153,40 W | 109,64 W | %71 |
| 0,34 Nm | 3480 d/d | 13,5 A | 13 V | 175,50 W | 123,91 W | %71 |
| 0,44 Nm | 3220 d/d | 16,9 A | 13 V | 219,70 W | 148,37 W | %68 |
| 0,50 Nm | 3190 d/d | 19,0 A | 13 V | 248,90 W | 167,04 W | %67 |
| 0,54 Nm | 3176 d/d | 20,2 A | 13 V | 274,72 W | 179,61 W | %65 |
| 0,64 Nm | 3300 d/d | 23,1 A | 13 V | 300,30 W | 221,18 W | %74 |
| 0,69 Nm | 2540 d/d | 26,1 A | 13 V | 334,08 W | 183,54 W | %55 |
| 0,79 Nm | 2380 d/d | 30,0 A | 13 V | 396,00 W | 196,90 W | %50 |
| 0,83 Nm | 2310 d/d | 31,2 A | 13 V | 424,32 W | 200,79 W | %47 |
| 0,89 Nm | 1862 d/d | 35,1 A | 13 V | 431,73 W | 173,55 W | %40 |
| 0,95 Nm | 1736 d/d | 38,4 A | 13 V | 503,04 W | 172,71 W | %34 |

Table 5: PWM frequency = 20 kHz

| Torque | Speed | Current | Voltage | P _{mec} | P _{elec} | Efficiency |
|---------|----------|---------|---------|------------------|-------------------|------------|
| 0,17 Nm | 3900 d/d | 8,6 A | 13 V | 112,66 W | 69,43 W | %62 |
| 0,27 Nm | 3680 d/d | 11,5 A | 13 V | 150,65 W | 104,05 W | %64 |
| 0,39 Nm | 3350 d/d | 15,4 A | 13 V | 200,20 W | 136,82 W | %68 |
| 0,49 Nm | 3250 d/d | 18,7 A | 13 V | 250,58 W | 166,77 W | %67 |
| 0,57 Nm | 2550 d/d | 23,4 A | 13 V | 285,48 W | 152,22 W | %53 |

The most important elements that affect the working performance and efficiency of FDAMs are motor driver board. However, the performance of these motor driver boards is determined by the switching circuits. The performance of motor driver boards with a correct switching circuit is quite high. Table 6 shows the data of the 24V BLDC motor where the algorithms are tested.

Table 6: 24v Brushless direct current motor features

| Parameter | Value | Unit |
|--|----------|------|
| Nominal Speed | 4000 | Rpm |
| Nominal Voltage | 24 | V |
| Stator Winding Factor | 0,866025 | |
| D-Axis Reactive Inductance L _{ad} | 2532,06 | nH |
| Q- Axis Reactive Inductance L _{aq} | 2532,06 | nH |
| D- Axis Inductance L _{1+l_{ad}} | 1295,9 | nH |
| Q- Axis Inductance L _{1+l_{aq}} | 1295,9 | nH |
| Armature Leakage Inductance L ₁ | 1042,9 | nH |
| Armature Phase Resistance R ₁ | 0.08489 | Ohm |
| D-Axis Time Constant (s) | 298319 | ns |
| Q-Axis Time Constant (s) | 298319 | ns |

Position information is obtained from hall-effect sensors. As explained in Table 1 and 2, the commutation order is determined and flux synchronization is performed. The signal to be applied to the switching elements is determined depending on the number of phases. Pulse width modulation (PWM) trigger signals are obtained with respect to the angles. Motor control is performed.

Table 7: Sensor positions and excited phases

| Hall-Effect Sensors | | | | Phase Outputs | | | | |
|---------------------|----|----|-----|---------------|-----|-----|-----|-----|
| HA | HB | HC | GLA | GLB | GLC | GHA | GHB | GHC |
| 1 | 0 | 1 | 1 | 0 | 0 | 0 | 0 | PWM |
| 1 | 0 | 0 | 0 | 1 | 0 | 0 | 0 | PWM |
| 1 | 1 | 0 | 0 | 1 | 0 | PWM | 0 | 0 |
| 0 | 1 | 0 | 0 | 0 | 1 | PWM | 0 | 0 |
| 0 | 1 | 1 | 0 | 0 | 1 | 0 | PWM | 0 |
| 0 | 0 | 1 | 1 | 0 | 0 | 0 | PWM | 0 |

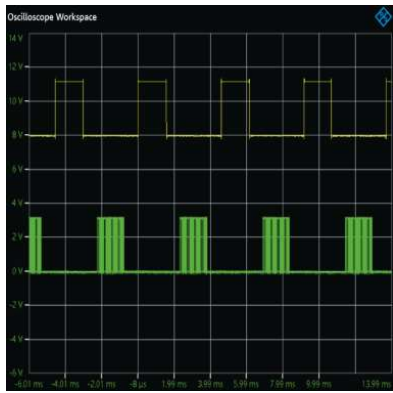


Figure 11: MOSFET Driver inputs



Figure 12: MOSFET Driver inputs

One electrical cycle must be completed for each rotor pole pair. In order to turn the motor clockwise or counter-clockwise, first of all, our position must be determined with the hall-effect sensor. The PWM signal is applied to the switches specified in the table. By continuing this cycle in this way, the motor is turned in the desired direction. The method applied in many sources is given in Table 7. Here, while PWM is applied to a MOSFET from the positive side, a logic signal is applied to a different phase on the negative side. Signals applied to the input of the MOSFET driver are shown in the Figure 11.

Table 8: Sensor positions and excited phases (inverse PWM = /PWM)

| Hall-Effect Sensors | | | Phase Outputs | | | | | |
|---------------------|----|----|---------------|------|------|-----|-----|-----|
| HA | HB | HC | GLA | GLB | GLC | GHA | GHB | GHC |
| 1 | 0 | 1 | 1 | 0 | /PWM | 0 | 0 | PWM |
| 1 | 0 | 0 | 0 | 1 | /PWM | 0 | 0 | PWM |
| 1 | 1 | 0 | /PWM | 1 | 0 | PWM | 0 | 0 |
| 0 | 1 | 0 | /PWM | 0 | 1 | PWM | 0 | 0 |
| 0 | 1 | 1 | 0 | /PWM | 1 | 0 | PWM | 0 |
| 0 | 0 | 1 | 1 | /PWM | 0 | 0 | PWM | 0 |

In Table 8, the reverse PWM signal is given together with the PWM signal. While the motor is driven with PWM over the MOSFET on the positive side of the phase, the phase is damped faster with inverse PWM. However, using reverse inverse PWM causes dead time problems. Therefore, the PWM rate decreases due to the dead time period left. The signals applied to the MOSFET driver input are given in the Figure 12. Related sensor rows are shown in the tables by applying the torque test on the motor.



Figure 13: MOSFET Driver inputs Dead-time

Along with PWM, the signal at the MOSFET driver inputs of the channels inverse PWM applied on the half bridge is given in Figure 13.

Table 9: 16 kHz %85PWM

| Torque | Speed | Current | Voltage | P _{mec} | P _{elec} | Efficiency |
|---------|------------|---------|---------|------------------|-------------------|------------|
| 0,12 Nm | 3730,0 rpm | 3,2 A | 26,1 V | 47 W | 84 W | %61,04 |
| 0,22 Nm | 3550,0 rpm | 4,6 A | 26,1 V | 82 W | 120 W | %74,09 |
| 0,27 Nm | 3447,0 rpm | 5,4 A | 26,1 V | 97 W | 141 W | %75,21 |
| 0,32 Nm | 3380,0 rpm | 5,9 A | 26,1 V | 113 W | 154 W | %80,00 |
| 0,37 Nm | 3308,0 rpm | 6,5 A | 26,1 V | 128 W | 170 W | %82,17 |
| 0,42 Nm | 3206,0 rpm | 7,2 A | 26,1 V | 141 W | 188 W | %81,61 |
| 0,52 Nm | 3050,0 rpm | 8,6 A | 26,1 V | 166 W | 224 W | %80,48 |
| 0,62 Nm | 2907,0 rpm | 9,9 A | 26,1 V | 189 W | 258 W | %79,45 |

Table 10: 16 kHz %85PWM inverse PWM

| Torque | Speed | Current | Voltage | P _{mec} | P _{elec} | Efficiency |
|---------|------------|---------|---------|------------------|-------------------|------------|
| 0,12 Nm | 3450,0 rpm | 3,2 A | 26,1 | 43 W | 84 W | %56,46 |
| 0,22 Nm | 3309,0 rpm | 4,6 A | 26,1 | 76 W | 120 W | %69,06 |
| 0,27 Nm | 3206,0 rpm | 5,4 A | 26,1 | 91 W | 141 W | %69,95 |
| 0,32 Nm | 3123,0 rpm | 6 A | 26,1 | 105 W | 157 W | %72,69 |
| 0,37 Nm | 3060,0 rpm | 6,6 A | 26,1 | 119 W | 172 W | %74,86 |
| 0,42 Nm | 2994,0 rpm | 7,2 A | 26,1 | 132 W | 188 W | %76,22 |
| 0,52 Nm | 2850,0 rpm | 8,4 A | 26,1 | 155 W | 219 W | %76,99 |
| 0,62 Nm | 2712,0 rpm | 9,8 A | 26,1 | 176 W | 256 W | %74,87 |

The data of the motor tested using the signals given in table 7 and table 8 are shown in table 9 and table 10. In these data, the PWM duty cycle input rate was kept constant. Current, speed, torque and efficiency will be considered for comparisons.

3. CONCLUSION

This study examines the frequency-dependent changes in the BLDCM driven by efficient, low-cost, and reliable use. To control the speed of the BLDCM, the PWM signal is applied to the switching elements of the relevant phases, depending on the rotor position information, and the motor is driven. The STM32F031 Microprocessor contains the Prescaler register for frequency changes together with its structure. The obtained results shows that the low frequency of the motor gives better results than the high frequency at the load start moments. In the load-balanced motor, providing the most optimal frequency should be a priority. The oscilloscope outputs of the current are shared while the motor is driven on the printed circuit board with the experimental demonstration results. Various graphs from 8kHz to 20kHz are given in the graphs taken from the oscilloscope. These graphs are given as phase ground and phase to phase. The switching frequency change is visible in the phase-ground plots. In this study, the motor dynamic model and the relationship between the inductance it contains and the switching frequency are included. 26V motor tests were performed by changing the switching method.

In many applications in the literature, reverse PWM signal is not used. In some applications, it is seen that PWM and reverse PWM signal are used together. As the dead time left between PWM signals increases, decreases in motor speed are observed. An increase in dead time means a decrease in the voltage falling on the motor. Therefore, speed and efficiency decrease. Signal shapes and graphics on the motor are shown. Reverse PWM is applied in the negative region of the conducting phase. Two different methods were compared. It was observed that the motor speed was higher when reverse PWM was not used. The data of the realized motor is shared. In order to better see the effects of the switching method and switching frequency, the tests on 26 V were done with %85 duty cycle. The data of the realized motor is shared. In this way, the sensor control of 13V BLDCM and the improvement of its load start by frequency are provided. Thus, the PWM frequency should be low at motor starting under the load, and it should be switched to high frequency after starting to reach steady state. Optimum switching mode and optimum frequency were tried to be determined. It has been shown to be more efficient starting at 10kHz with 15kHz at rated load.

4. REFERENCES

1. Bekiroglu, E., Dalkin, A. (2020). Comparison of Trapezoidal and Sinusoidal PWM Techniques for Speed and Position Control of PMSM. *Advances in Electrical and Electronic Engineering*, 18(4), 207-216.
2. Ctibor, J., Vorel, P., Knobloch, J., & Pazdera, I. (2019). BLDC Motor Control with Cascade Structure Utilizing ARM MCU. *IEEE International Conference on Electrical Drives & Power Electronics (EDPE)* pp. 61-65
3. Echle, A., Gong, Y., Terfurth, J., & Parspour, N. (2020). FEA-Based Comparison of BLDC and BLAC Modes for an Axial Flux Motor with Trapezoidal BEMF. In *IECON 2020 The 46th Annual Conference of the IEEE Industrial Electronics Society* (pp. 2694-2701). IEEE.
4. Kolano, K., Drzymała, B., & Gęca, J. (2021). Sinusoidal Control of a Brushless DC Motor with Misalignment of Hall Sensors. *Energies*, 14(13), 3845.
5. Papathanasopoulos, D. A., Mitronikas, E. D., Giannousakis, K. N., & Dermatas, E. S. (2020). An Alternative Approach for Condition Monitoring of Brushless DC Motor Drives. In *2020 International Conference on Electrical Machines (ICEM)* (Vol. 1, pp. 1280-1286). IEEE.
6. Pindoriya, R. M., Mishra, A. K., Rajpurohit, B. S., & Kumar, R. (2018). FPGA-based digital control technique for BLDC motor drive. In *2018 IEEE Power & Energy Society General Meeting (PESGM)* (pp. 1-5). IEEE.
7. Su, Z., Xiao, Y., & Zhang, Y. (2019). The Design of the orchard spraying control system is based on STM32. In *2019 IEEE 3rd Advanced Information Management, Communicates, Electronic and Automation Control Conference (IMCEC)* (pp. 799-803). IEEE
8. Zhang, F., Kong, X., Li, F., & Zhang, Y. (2020). The Design of Controller for BLDC Based on STM32. In *IOP Conference Series: Earth and Environmental Science* (Vol. 446, No. 4, p. 042047). IOP Publishing.

Acknowledge:

- This publication was obtained from the KORMAS R&D studies within the scope of the "Brushless Direct Current Motor Magnetic Coupling Pump Design" project numbered 7190809, which was supported by TUBITAK (The Scientific and Technological Research Council of Turkey)
- In Turkish digest version of this study was presented in BILMES Congress in December 2021